

Multi-Band mm-Wave Antenna for 5G-WiGig Communication Systems

Nada Abdelatif^{1, *}, Hany Zamel¹, Ahmed Attiya¹, and Amr Awamry²

Abstract—In this paper, we develop a multi-band circularly polarized planar antenna operating at 28 GHz and 60 GHz for 5G and WiGig applications. The antenna is composed of a square slot antenna fed by a proximity coupled microstrip line and loaded by grounded square loop and three tilted angle strips. Grounded square patch introduces resonance at 60 GHz frequency while the strips introduce resonances at 28 GHz. The square slot is designed as a wide-band antenna which can support these two resonances.

1. INTRODUCTION

This paper introduces a novel design of a millimeter wave antenna which can be useful for a variety of applications, including transmission of large amounts of data and cellular communications [1–5]. As an example, Gigabit wireless communications require a considerable amount of bandwidth, which can only be supported by millimeter waves. WiGig represents the next-generation communications for WLAN and wireless personal network (WPAN). The standard of 802.11ad is set for WiGig at 60 GHz where the proposed system can provide a transmission rate of multi-gigabit [6, 7]. On the other hand, mm-wave frequency bands around 28 GHz, 38 GHz, and 73 GHz are already under consideration for future fifth-generation (5G) wireless technologies.

Recently, different multiband antenna configurations for 28/38 GHz have been demonstrated for 5G applications [5, 8]. On the other hand 60 GHz antennas which can be suitable for WiGig communication are discussed in [8–10]. The 60 GHz band supports the Wi-Fi and WiGig standard IEEE 802.11ad. The 5G and WiGig provide a 7 Gbit/s data rate transfer at 60 GHz and minimize the interference volume [6, 8].

In this paper we present a multi-band mm-wave antenna which can be used to combine 5G and WiGig applications in a handset like mobile phone or tablet. Circularly polarized antenna is preferred to avoid polarization misalignment in mobile applications [11]. The proposed antenna is composed of a wideband square slot antenna fed by a coupled microstrip line. In printed antenna structures like square or circular shapes with a single feeding point, a diagonal perturbation would introduce two orthogonal modes along the diagonals of these shape. As examples of these diagonal perturbations are triangular cuts on two opposite corners of a square patch or small open stubs on a circular patch [12]. By adjusting these diagonal perturbations, the two introduced orthogonal modes would have equal amplitudes and a phase shift of $\pm 90^\circ$ which introduce circular polarizations. In the present case, this perturbation is introduced inside the square slot. Thus, an appropriate choice to introduce a diagonal perturbation inside a square slot is to add diagonally tilted strips inside the loop. By adjusting the number, lengths, widths and spacing distances between these strips, it would be possible to adjust the required orthogonal mode. Since the lengths of the strips inside the loop are long enough to introduce this perturbation at

Received 18 December 2019, Accepted 22 January 2020, Scheduled 3 February 2020

* Corresponding author: Nada Abdelatif (nada.abdelatif@gmail.com).

¹ Electronics Research Institute (ERI), Cairo, Egypt. ² Electronics and Communication Engineering Department, Faculty of Engineering, Benha University, Benha, Kaliopia, Egypt.

the lower band, these strips are used to adjust the circular polarization at 28 GHz. On the other hand, smaller perturbations including a small loop and a small patch at the corners of the slot are used to introduce the required perturbation at the higher band at 60 GHz.

In Section 2 we present the analysis and design of the proposed antenna. Section 3 presents the current distributions and radiation patterns of the proposed antenna. The present simulations are obtained by using ANSYS HFSS. Section 4 proposes an experimental results of the proposed antenna. Finally, Section 5 presents the conclusion of our design.

2. ANALYSIS AND DESIGN

The proposed antenna is designed on a low loss substrate Rogers RO4003 with substrate thickness $h = 0.2$ mm and a dielectric constant of $\epsilon_r = 3.55$. The loss tangent of the substrate is 0.0027. For this substrate parameters, the width of a 50Ω microstrip line is $W_F = 0.4$ mm. The maximum operating frequency of this feeding microstrip line to avoid higher order modes is given by [13]:

$$f_T \cong \frac{c}{\sqrt{\epsilon_r}(2W_F + h)} \quad (1)$$

For the present case, this cutoff frequency is nearly 159 GHz. Other formulas for other higher order modes are discussed in [13]. However, the present one in Eq. (1) represents the lowest higher order mode in the present case. Thus, the obtained substrate parameters are suitable for the proposed operating frequency up to 60 GHz without introducing higher order modes.

The length of the square substrate layer is $L = 12$ mm. Figure 1(a) shows the starting design of the proposed antenna. It consists of a square slot on a partially grounded substrate and excited by a proximity coupled microstrip line on the other side of the substrate. The main radiation mechanism is due to the current on the inner edges of the square slot. The effective relative permittivity in the slot region is nearly given by:

$$\epsilon_{r_eff} \cong \frac{\epsilon_r + 1}{2} \quad (2)$$

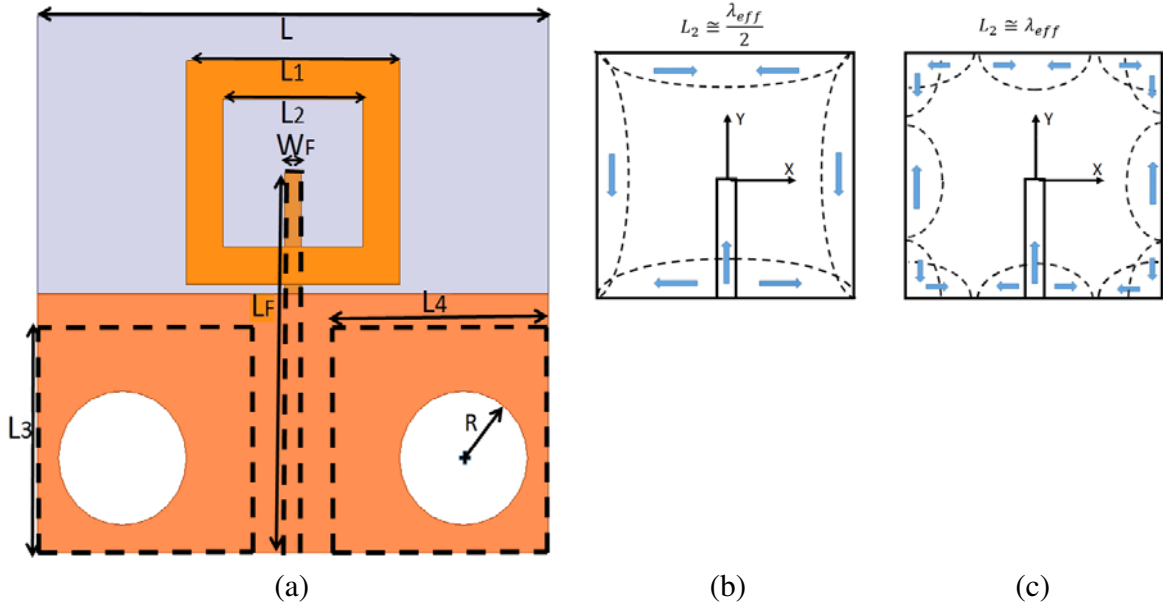


Figure 1. (a) Geometry of the proposed proximity-fed square loop antenna on a partially grounded substrate. Dashed lines represent the geometry of the lower structure. (b) Approximate current distribution along the edges of the inner slot at $L_2 \cong \frac{\lambda_{eff}}{2}$. (c) Approximate current distribution along the edges of the inner slot at $L_2 \cong \lambda_{eff}$.

Thus, the effective wave length at 28 GHz is nearly 6.4 mm and at 60 GHz is nearly 3 mm. For such slot structure the current dominates near the edges of the square slot. Hence, the length L_2 plays a critical role in the design of this square slot antenna. An appropriate choice for $L_2 \cong \lambda_{eff}/2$. In this case, the current distribution along the edges of the slot would be as shown in Figure 1(b). In this case, the current distributions along the edges parallel to the y -axis are the dominant in the radiation mechanism. On the other hand, when $L_2 \cong \lambda_{eff}$, the current distribution along the edges of the slot would be approximately as shown in Figure 1(c). In this case, the current components in each edge are in opposite directions. However, it can be expected that due, to the radiation effect, the amplitude of the current distribution along the edges parallel to the y -axis and at the corners near to the feeding line would be greater than the corresponding currents at the upper corners. Thus, the radiated fields due to the currents along the edges parallel to the y -axis do not vanish due to the opposite components as in the case of the edges parallel to the x -axis. Thus, according to this, the initial value of L_2 in the present analysis is set at 3.1 mm to approximately satisfy the condition of $\lambda_{eff}/2$ at 28 GHz and λ_{eff} at 60 GHz. The remaining dimensions of the proposed design including R , L_3 and L_4 are chosen based on the dimensions of the launcher connector of type 1.85 mm which is used in the experimental verification. By using numerical simulation of the proposed antenna structure, the dimensions of the square slot and the other parts of this antenna are optimized to introduce a matched antenna around the required operating frequency bands as presented in Table 1.

Figure 2 shows the reflection coefficient of this antenna structure in frequency band from 25 GHz to 65 GHz. It can be noted that this preliminarily design is matched in the frequency bands from 27 GHz to 37 GHz and from 56 GHz to 65 GHz. This antenna configuration is basically linear antenna.

To introduce circular polarization, it is required to add a perturbation along the diagonal of the square loop antenna. A smaller square loop is added at the layer of the feeding microstrip line as shown in Figure 3. The outer length of this square loop is $L_5 = 1.3$ mm and the width of its arm is 0.282 mm. The distances of this perturbation square loop from the outer corners of the square loop antenna are $X_a = -2.15$ mm and $Y_a = -1.68$ mm.

Figure 4 shows the reflection coefficients of this combined antenna structure at both lower and upper frequency bands. It can be noted that the presence of this ground square slot improves the matching at the lower frequency band. On the other hand, Figure 5 shows the corresponding axial ratio of this antenna structure. It can be noted that the axial ratio in this case is dropped around 28 GHz, but it is still greater than 3 dB. Thus, it is still required to adjust this diagonal perturbation to reduce the axial ratio at the 28 GHz band.

To improve the circular polarization, three additional tilted strips are added inside the square

Table 1. Dimensions in (mm) of initial design of square loop antenna.

L_1	L_2	L_3	L_F	W_F	R	L_4
5	3.3	5.8	8.5	0.4	1.5	5.08

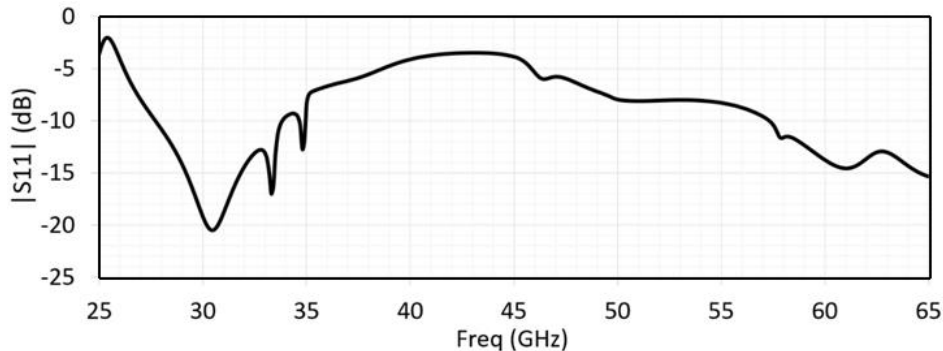


Figure 2. Reflection coefficient of the antenna shown in Figure 1.

aperture as shown in Figure 6. These three strips are tilted by an 45° angle anti clock wise. The width of these strips arms are $w_{st1} = 0.238$ mm. The lengths of two outer strips are $l_{st1} = 2.4$ mm while the length of the middle strip is $l_{st0} = 3.3$ mm. The gap distance between the adjacent strips is $g = 0.5$ mm.

Figure 7 shows the reflection coefficient of the antenna with the tilted strips. The reflection coefficient of the antenna after adding strips is improved antenna at lower frequency. However, the

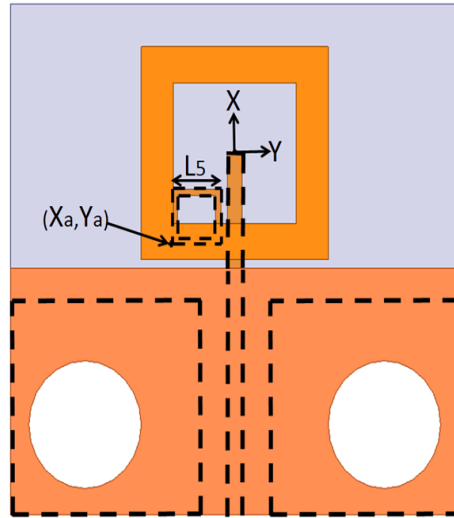


Figure 3. A small perturbation-square loop is added to the antenna structure at the lower side.

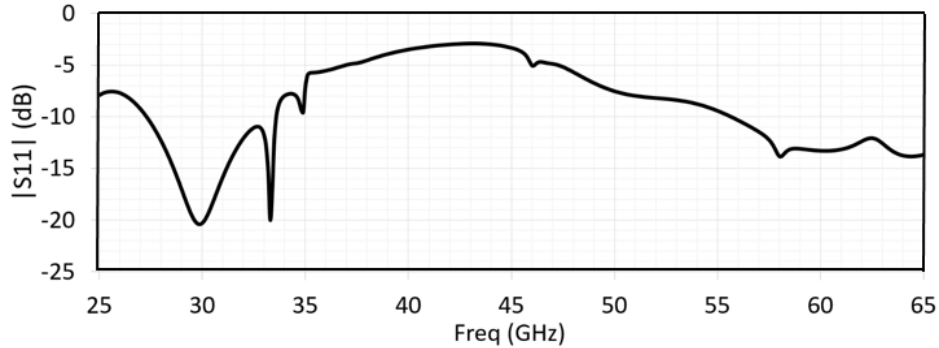


Figure 4. Reflection coefficient of the proposed antenna with the perturbing small loop.

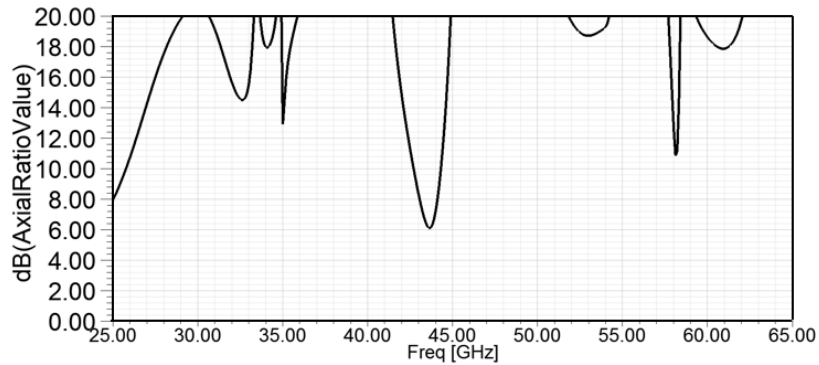


Figure 5. Axial ratio of the proposed antenna with the perturbing small loop.

reflection coefficient of the antenna at upper frequency still requires to be improved. The axial ratio of the antenna after adding the tilted strips is improved around 60 GHz frequency and 28 GHz too as shown in Figure 8. However, the required axial ratios at the required frequencies still need to be improved.

To improve the reflection coefficient at the upper frequency, an open circuit tuning stub is used as shown in Figure 9. The tuning stub is added to the right of the coupled microstrip line at a distance $L_d = 7.9$ mm from the feeding point. The dimensions of the tuning stub are $L_{st} = 0.4$ mm and $W_{st} = 0.5$ mm. Figure 10 shows the reflection coefficient after adding this matching stub. It can be noted that this stub extends the upper frequency. On the other hand, Figure 11 shows the corresponding

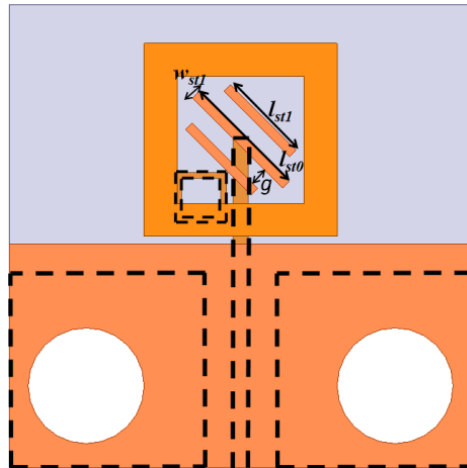


Figure 6. The proposed antenna with perturbing small square loop and tilted strips.

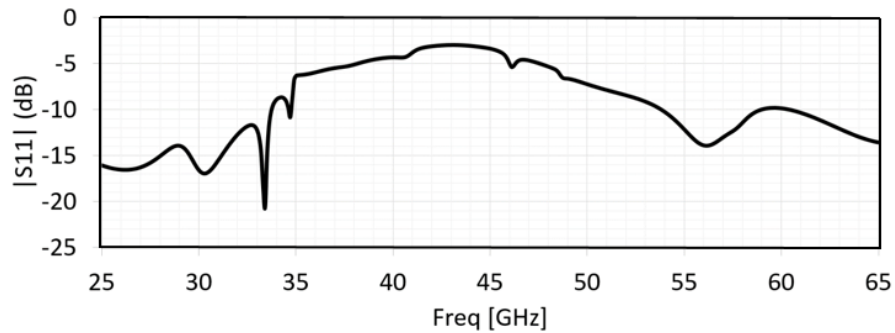


Figure 7. Reflection coefficient of the proposed antenna with perturbing small square loop and tilted strips.

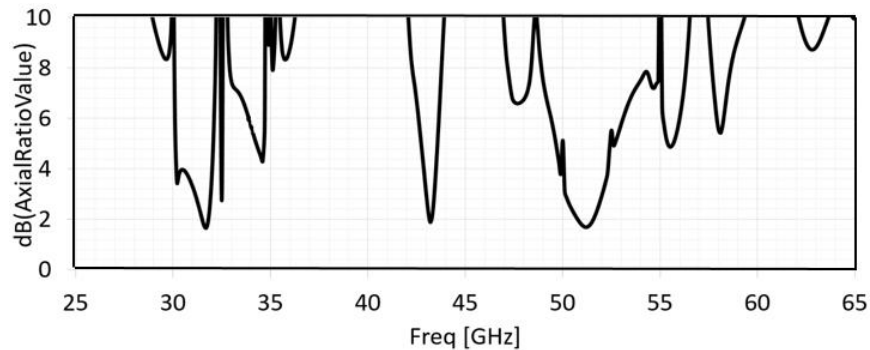


Figure 8. Axial ratio of the proposed antenna with perturbing small square loop and tilted strips.

axial ratio of the antenna structure.

To introduce circular polarization at the upper frequency band around 60 GHz, it is required to add another perturbation along the diagonal of the square loop antenna. A small square patch is added at the lower plane of the antenna as shown in Figure 12. The length of this small square patch is $l_6 = 1$ mm. The lower left corner of this square patch is located at $X_b = 0.32$ mm and $Y_b = 0.75$ mm. Figure 13 shows the reflection coefficients of this combined antenna structure at both lower and upper frequency bands. Figure 14 show the corresponding axial ratio of this antenna structure.

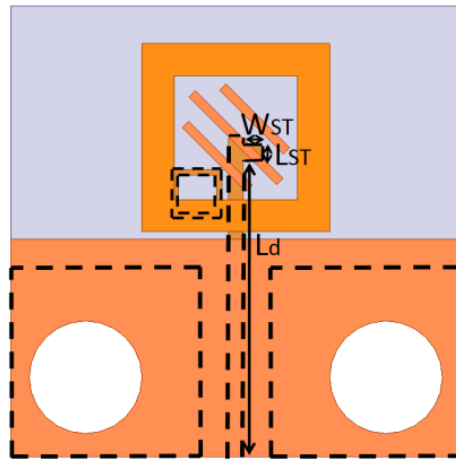


Figure 9. The proposed antenna with a tuning stub on the feeding line.

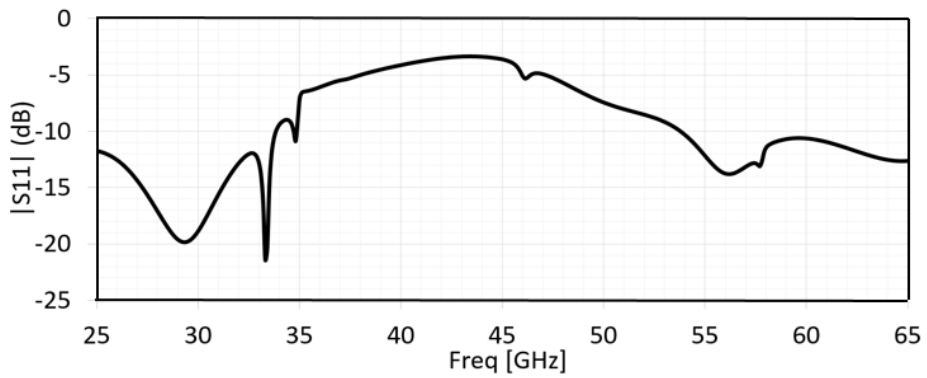


Figure 10. Reflection coefficient of the antenna with the tuning stub.

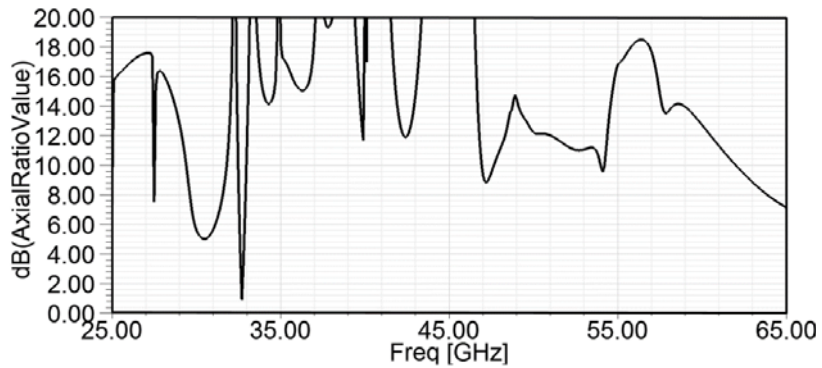


Figure 11. Axial ratio of the antenna with the tuning stub.

To adjust the axial ratios at the required frequency bands, two triangles are subtracted from the perturbation square patch as shown in Figure 15. The length L_p is 0.495 mm. The reflection coefficient is adjusted at both 28 and 60 GHz by this modification as shown in Figure 16 compared to the corresponding result shown in Figure 13. In addition, the axial ratio is quite improved as shown in Figure 16.

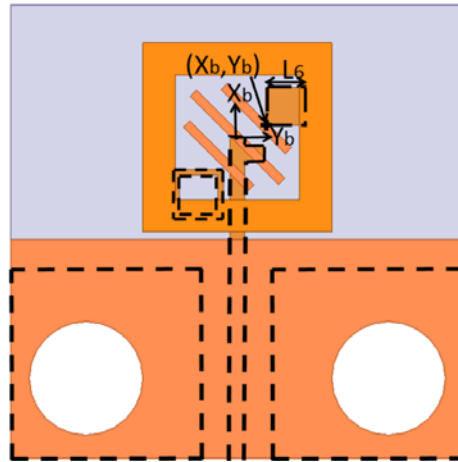


Figure 12. The proposed antenna with a square patch perturbation in the lower plane of the antenna.

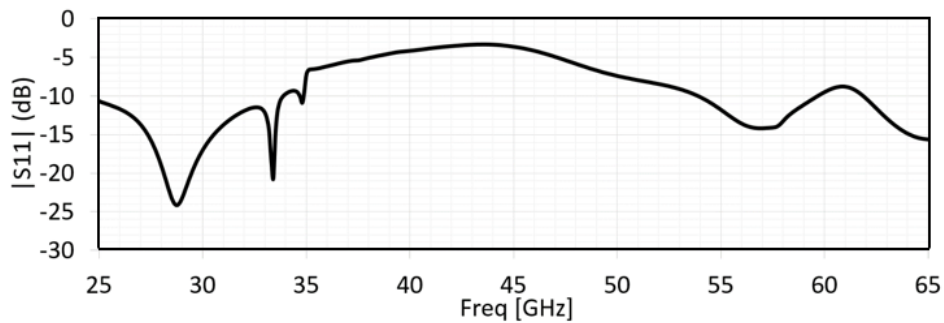


Figure 13. Reflection coefficient of the antenna with the square patch perturbation.

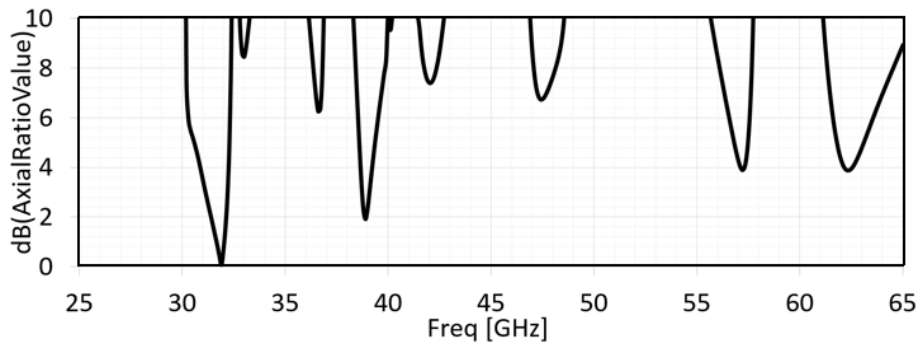


Figure 14. Axial ratio of the antenna with the square patch perturbation.

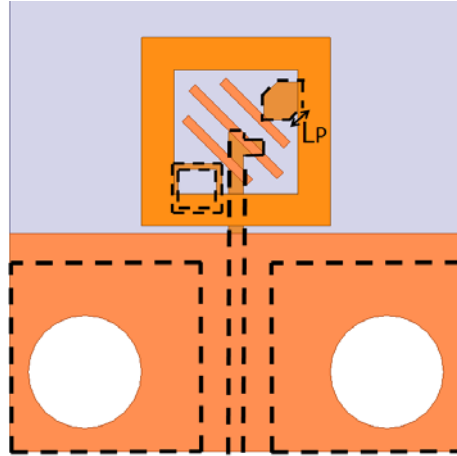


Figure 15. Cutting the corner out of the ground square patch of the antenna.

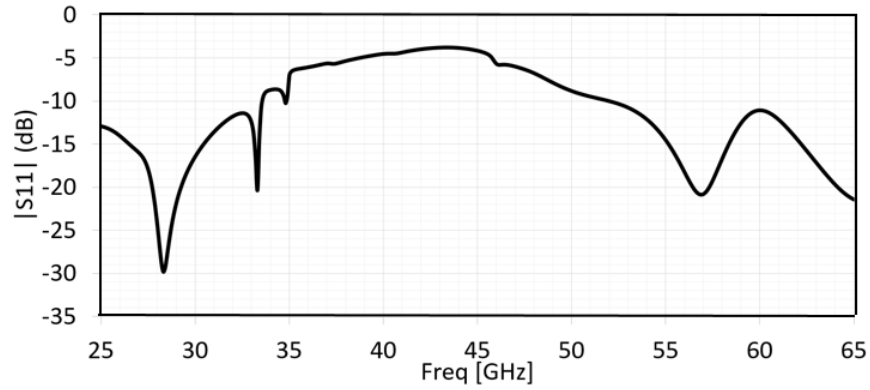


Figure 16. Reflection coefficient of the complete antenna design.

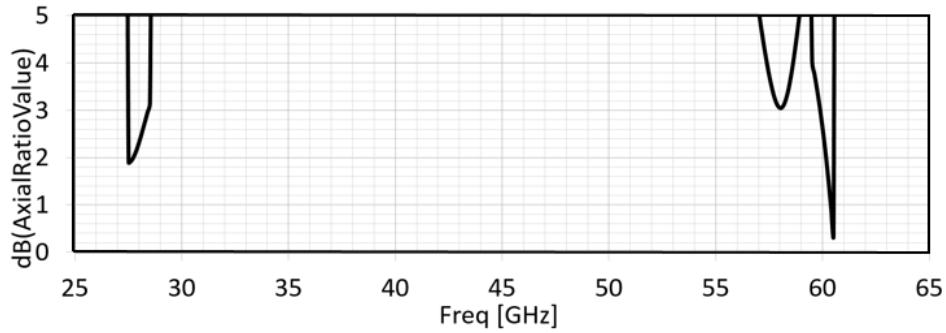


Figure 17. Axial ratio of the complete antenna design.

3. CURRENT DISTRIBUTIONS AND RADIATION PATTERN

The simulated surface current distributions at the two bands of the antenna design are shown at Figure 18. The current at 28 GHz is mainly distributed on the middle strip and the current vector rotate counterclockwise as shown in Figure 18(a), where the current on the middle strip contributes to the right-hand circular polarized (RHCP) radiation at the lower band. Similarly, the strips generates left-hand circular polarized (LHCP) radiation at the upper band as shown in Figure 18(b). Strong coupling between the square loop patches is observed since most energy is coupled to microstrip line

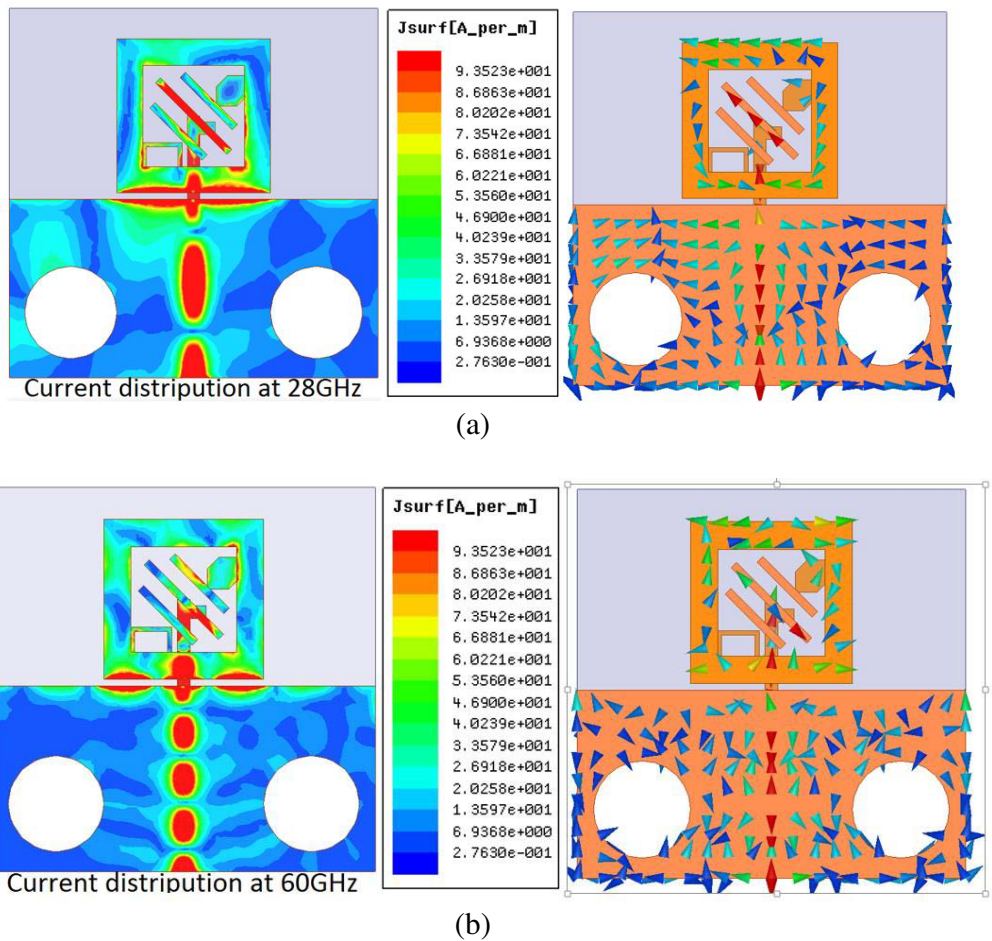


Figure 18. Simulated current distributions on the circular two ring radiator at (a) 28 GHz, and (b) 60 GHz.

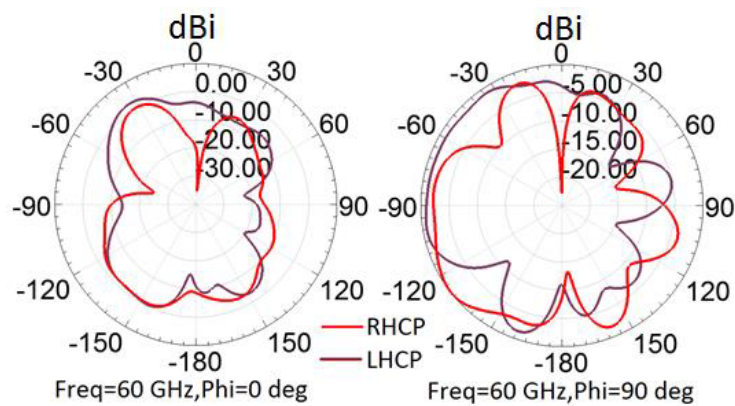


Figure 19. Simulated gain radiation pattern of the proposed antenna for LHCP, RHCP at 60 GHz for $\varphi = 0^\circ$ and 90° .

and the connector at both bands.

The simulated radiation pattern of the proposed antenna for LHCP, RHCP at 28 GHz and 60 GHz for $\varphi = 0^\circ$ and 90° is shown in Figures 19 and 20. It is clear that the proposed antenna presents good broadside radiation patterns.

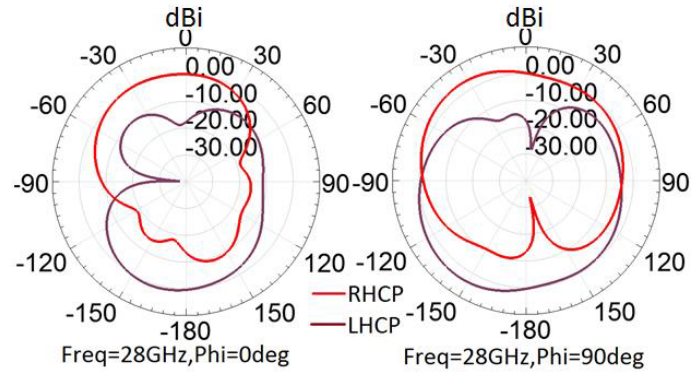


Figure 20. Simulated gain radiation pattern of the proposed antenna for LHCP, RHCP at 28 GHz for $\varphi = 0^\circ$ and 90° .

4. EXPERIMENTAL RESULTS

The proposed multi-band antenna is fabricated and measured using an Agilent R&S ZVA67 Vector Network Analyzer. The fabricated images of the top and bottom views of the proposed antenna are represented in Figures 21(a) and 21(b), respectively.

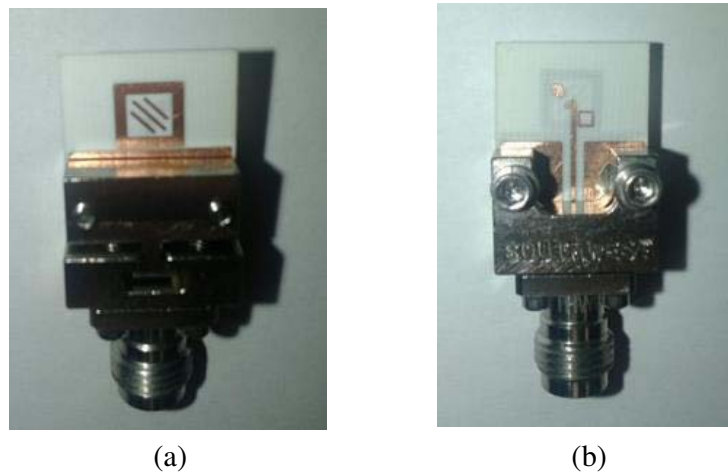


Figure 21. Fabricated prototypes of the proposed antenna; (a) top view, (b) bottom view.

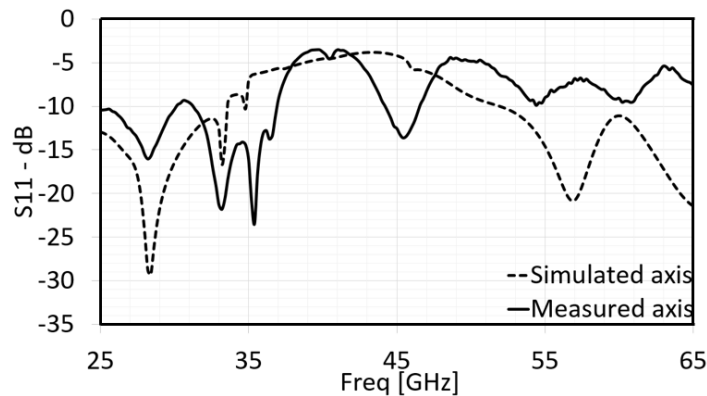


Figure 22. Measured and simulated reflection coefficients.

The measured and simulated return losses against frequency are shown in Figure 22. It can be seen that good agreement is obtained between the measured and simulated values. The slight differences are due to fabrication tolerances.

5. CONCLUSION

The analysis and design of a dual-band CP microstrip antenna for 28 and 60 GHz bands is proposed. The antenna consists of a square loop on a partially grounded substrate and is excited by a proximity coupled microstrip line on the other side of the substrate. A small square patch is added to the ground plane of the antenna to introduce the 60 GHz frequency. Three tilted angle strips and small grounded square loop are added to improve the circular polarization of the antenna. The simulated minimum AR values at the two bands (28 and 60 GHz) are 2.2 and 2.7 dB, and the 3-dB axial ratio bandwidths are 0.918 GHz (3.2%) and 0.6633 GHz (1.1%), respectively. The proposed antenna can be used in several wireless communication applications such as 5G and WiGig applications.

REFERENCES

1. Kulemin, G. and D. Barton, *Millimeter-Wave Radar Targets and Clutter*, Artech House, 2003.
2. Preez, J. and S. Sinha, *Millimeter-Wave Antennas: Configurations and Applications*, Springer, 2016.
3. Huang, K. and Z. Wang, *Millimeter Wave Communication Systems*, John Wiley & Sons, 2011.
4. Niu, Y., Y. Li, D. Jin, L. Su, and A. Vasilakos, "A survey of millimeter wave communications (mm-wave) for 5G: Opportunities and challenges," *Wireless Networks*, Vol. 21, No. 8, 2657–2676, 2015.
5. Hashem, Y., O. Haraz, and E. El-Sayed, "6-element 28/38 GHz dual-band MIMO PIFA for future 5G cellular systems," *IEEE Int. Symp. on Ant. and Prop.*, 393–394, 2016.
6. Wang, D. and C. Chan, "Multiband antenna for Wi-Fi and WiGig communications," *IEEE Ant. and Wireless Prop. Lett.*, Vol. 15, 309–312, 2016.
7. Nguyen, K., M. Kibria, K. Ishizu, and F. Kojima, "Feasibility study of providing backward compatibility with MPTCP to WiGig/IEEE 802.11 ad," *IEEE 86th Vehicular Technology Conference*, 1–5, 2017.
8. Ali, M. and A. Sebak, "Dual band (28/38 GHz) CPW slot directive antenna for future 5G cellular applications," *IEEE Int. Sym. on Ant. and Prop.*, 399–400, 2016.
9. Bisognin, A., D. Titz, C. Luxey, G. Jacquemod, A. Bisognin, R. Pilard, F. Gianesello, D. Gloria, and L. Claire, "Millimeter-wave antenna-in-package solutions for WiGig and backhaul applications," *IEEE Int. Workshop on Ant. Technology (iWAT)*, 52–55, 2015.
10. Ibrahim, M., "Low-cost, circularly polarized, and wideband U-slot microstrip patch antenna with parasitic elements for WiGig and WPAN applications," *13th European Con. on Ant. and Prop. (EuCAP)*, 1–4, 2019.
11. Paul, P., K. Kandasamy, and M. S. Sharawi, "A triband circularly polarized strip and SRR-loaded slot antenna," *IEEE Trans. on Ant. and Prop.*, Vol. 66, 5569–5573, 2018.
12. James, J. R. and P. S. Hall, "Circular polarisation and bandwidth," *Handbook of Microstrip Antennas*, Ch. 4, Peter Peregrinus Ltd., 1989.
13. Pozar, D. M., *Microwave Engineering*, 4th Edition, John Wiley & Sons, 2011.